Computers and Concrete, *Vol. 12, No. 5 (2013) 585-612*
DOI: http://dx.doi.org/10.12989/cac.2013.12.5.585

Modelling reinforced concrete beams under mixed shear-tension failure with different continuous FE approaches

Ireneusz Marzec*, Łukasz Skarżyński[a], Jerzy Bobiński[b] and Jacek Tejchman[c]

Department of Civil Engineering, Gdansk University of Technology, Gdansk, Narutowicza 11/12, Poland

(*Received February 17, 2012, Revised April 18, 2013, Accepted May 8, 2013*)

Abstract. The paper presents quasi-static numerical simulations of the behaviour of short reinforced concrete beams without shear reinforcement under mixed shear-tension failure using the FEM and four various constitutive continuum models for concrete. First, an isotropic elasto-plastic model with a Drucker-Prager criterion defined in compression and with a Rankine criterion defined in tension was used. Next, an anisotropic smeared crack and isotropic damage model were applied. Finally, an elasto-plastic-damage model was used. To ensure mesh-independent FE results, to describe strain localization in concrete and to capture a deterministic size effect, all models were enhanced in a softening regime by a characteristic length of micro-structure by means of a non-local theory. Bond-slip between concrete and reinforcement was considered. The numerical results were directly compared with the corresponding laboratory tests performed by Walraven and Lehwalter (1994). The advantages and disadvantages of enhanced models to model the reinforced concrete behaviour were outlined.

Keywords: bond-slip; characteristic length; damage mechanics; elasto-plasticity; non-local theory; reinforced concrete beam; size effect; smeared crack model; strain localization

1. Introduction

Modelling of concrete structures has to include a fracture process, which is a fundamental phenomenon in all quasi-brittle materials (Bažant and Planas 1998). It is a major reason of their damage under mechanical loading contributing to a significant degradation of the material strength which may lead to a total loss of load-bearing capacity. During fracture first micro-cracks arise which change gradually into dominant macroscopic discrete cracks up to rupture. Thus, a fracture process may be subdivided in general into two main stages: a) appearance of narrow localized zones of intense deformation including micro-cracks and b) occurrence of discrete macro-cracks. Within continuum mechanics, strain localization should be numerically captured by a continuous approach and discrete macro-cracks by a discontinuous one, e.g. XFEM (Meschke and Dumstorff 2007, Tejchman and Bobiński 2013). Usually, to describe the fracture behaviour of concrete, one

*Corresponding author, Ph. D., E-mail: irek@pg.gda.pl
[a]Ph. D., E-mail: lskarzyn@pg.gda.pl
[b]Ph. D., E-mail: bobin@pg.gda.pl
[c] Professor, E-mail: tejchmk@pg.gda.pl

http://www.techno-press.org/?journal=cac&subpage=8 ISSN: 1598-8198 (Print), 1598-818X (Online)

approach is used. However, in order to describe the entire fracture process, a continuous approach should be connected with a discontinuous one (Moonen *et al.* 2008, Bobiński and Tejchman 2013).

In our paper, we deal solely with a continuous approach. Continuum models describing the mechanical behaviour of concrete were formulated within, among others, endochronic approach (Bažant and Bhat 1976), rate-independent plasticity (Pietruszczak *et al.* 1988, Menetrey and Willam 1995), damage theory (Dragon and Mróz 1979, Ragueneau *et al.* 2000), coupled damage and plasticity (de Borst *et al*. 1999, Ibrahimbegovic *et al*. 2003), micro-plane theory (Bažant and Ožbolt 1990, Jirásek 1999) and smeared crack approach (Jirásek and Zimmermann 1998, Souza 2010). To properly model the thickness and spacing of localized zones, continuum models require an extension in the form of a characteristic length. Such an extension can be done with strain gradient (Pamin and de Borst 1999), viscous (Sluys and de Borst 1994) and non-local terms (Pijaudier-Cabot and Bažant 1987). To simulate reinforced concrete elements, Cervenka and Papanikolau (2008) proposed a continuum fracture-plastic approach. In turn, Oliver *et al.* (2008) used a Strong Discontinuity Approach (SDA) and Rabczuk *et al.* (2008) developed a cohesive particle method.

The intention of our paper is to check the capability of different enhanced continuum constitutive models for concrete to describe strain localization and related deterministic size effect in concrete beams with longitudinal reinforcement and without stirrups subjected to mixed shear-tension failure using the FEM. The models are relatively simple and can be implemented into commercial FE codes. First, an isotropic elasto-plastic model with a Drucker-Prager criterion defined in compression and with a Rankine criterion defined in tension was used (model ‘1’). Next, an isotropic damage model (model ‘2’) and an anisotropic smeared crack model (model ‘3’) were applied. Finally, a coupled elasto-plastic-damage formulation based on the strain equivalence hypothesis was used (model ‘4’). To ensure mesh-independent FE results, to describe strain localization in concrete and to capture a deterministic size effect, all models were enhanced in a softening regime by a characteristic length of micro-structure by means of a non-local theory (Pijauder-Cabot and Bažant 1987, Bažant and Jirásek 2002, Bobiński and Tejchman 2004). To simulate the behaviour of reinforcement, an associated elasto-perfectly plastic constitutive law was assumed. A bond-slip law between concrete and reinforcement was considered (Dörr 1980, den Uijl and Bigaj 1996). Numerical results were compared with corresponding laboratory tests by Walraven and Lehwalter (1994), i.e., with the results of the measured load bearing capacity of beams and observed patterns of cracks (the experimental force-displacement diagrams were not enclosed). Just recently these laboratory experiments were simulated by Ooi and Yang (2011) using a hybrid finite element-scaled boundary element method.

The paper is a continuation of our earlier numerical studies on the behaviour of reinforced concrete corbels with 3 different continuum approaches (Syroka *et al.* 2011), where a mixed tensile-shear failure was also a dominating mechanism. An isotropic elasto-plastic, isotropic damage with 2 definitions of the equivalent strain measure and smeared crack constitutive model (with rotating and fixed cracks) with non-local softening were used. The best agreement with experimental load-displacement diagrams was obtained using the elasto-plastic and isotropic damage model with non-local softening. The ultimate forces calculated using the elasto-plastic and isotropic damage models were both 20% higher than the experimental values whereas the calculated ones using the anisotropic smeared crack model were higher by 45%. Concerning the simulated geometry of localized zones, the most satisfactory agreement was achieved again with the elasto-plastic model, next with the damage model and finally with the smeared fixed crack model.

The innovative points in this paper concern a comparative application of 4 different enhanced continuum approaches to describe a pattern of localized zones and a related deterministic size effect (isotropic elasto-plastic, isotropic damage with 3 definitions of the equivalent strain measure, combined elasto-plastic-damage model and smeared crack constitutive model with rotating and fixed cracks in reinforced concrete beams of a different size where a mixed shear-tension type of failure occurred (note that most FE solutions for reinforced concrete beams concern a tension type of failure).

2. Experiments on reinforced concrete beams

Laboratory tests were carried out on five different short reinforced concrete beams without shear reinforcement (Walraven and Lehwalter 1994). The geometry of the beams is shown in Fig. 1 and Table 1. The beams were freely supported. The beam length L varied between 680 mm and 2250 mm and the height h was between 200 mm and 1000 mm (the beams' width b was always 250 mm). The ratio between the width of the loading plate k and the effective beam depth d was kept constant (k/d = 0.25). The maximum aggregate size in concrete was d_{max} = 16 mm. The concrete cover measured from the bar centre to the concrete surface was 40 mm for the smallest beam and 70 mm for the largest one. In the tests, the span-to-depth ratio was always L_t/d = 1. The cylinder compressive strength of concrete was about f_c = 20 MPa. In turn, the cylinder splitting tensile strength of concrete was about f_t = 2 MPa. The longitudinal reinforcement ratio of the specimens was 1.1% (yield strength was 420 MPa). To obtain a geometrically similar cross-sectional area, various combinations of bar sizes were used (with the diameter of 16, 18 and 20 mm). The beams were incrementally loaded by a vertical force applied at a mid-span of each beam. During loading, first, at about 40% of the failure load, bending cracks appeared. Afterwards, at about 45-50% of the failure load, the first inclined crack occurred. The beam failure took place in a gradual gentle way in shear compression by crushing concrete adjacent to the loading plate initiated by a formation of short parallel inclined cracks.

A pronounced size effect was observed in tests exemplified by the reduction of the nominal normalized shear strength $v_u = V_u/(bdf_c)$ with increasing effective cross sectional depth d in the range of beam heights h = 200-800 mm: v_u = 0.23 (h = 200 mm), v_u = 0.15 (h = 400 mm), v_u = 0.13 (h = 600 mm), v_u = 0.10 (h = 800-1000 mm) (V_u - maximum shear force in Table 1). The cracks developed significantly faster in the larger beams.

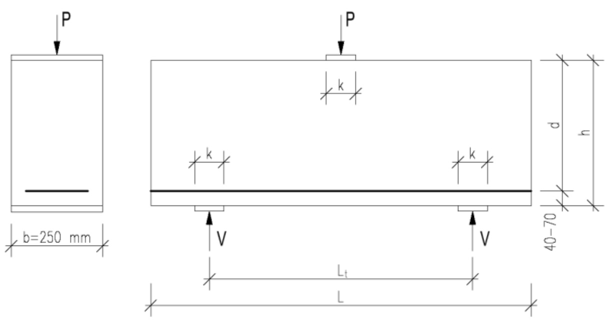

Fig. 1 Geometry of reinforced concrete beams used in laboratory tests by Walraven and Lehwalter (1994)

Table 1 Properties of reinforced concrete beams of Fig. 1 and experimental failure vertical force

Beam	h [mm]	d [mm]	L_t [mm]	L [mm]	A_{sl} [mm^2]	bars	f_c [N/mm^2]	V_u [kN]
V711	200	160	320	680	606	3ø16	18.1	165
V022	400	360	720	1030	1020	4ø18	19.9	270
V511	600	560	1120	1380	1570	5ø20	19.8	350
V411	800	740	1480	1780	2040	2 (4ø18)	19.4	365
V211	1000	930	1860	2250	2510	2 (4ø18)	20.0	505

3. Constitutive models

3.1 Isotropic elasto-plastic model for concrete

In a compression regime, a shear yield surface based on the linear Drucker-Prager criterion with isotropic hardening and softening was used (Marzec *et al.* 2007, Majewski *et al.* 2008, Tejchman and Bobiński 2013)

$$f_1 = q + p\tan\varphi - \left(1 - \frac{1}{3}\tan\varphi\right)\sigma_c(\kappa_1) \tag{1}$$

where q is the Mises equivalent deviatoric stress, p denotes the mean stress and φ is the internal friction angle. The evolution of material hardening/softening was defined by the uniaxial compression yield stress $\sigma_c(\kappa_1)$. The internal friction angle φ was assumed as

$$\tan\varphi = \frac{3\left(1 - r_{bc}^{\sigma}\right)}{1 - 2r_{bc}^{\sigma}} \tag{2}$$

where r_{bc}^{σ} is the ratio between the biaxial compressive strength and uniaxial compressive strength ($r_{bc}^{\sigma} = 1.2$). The invariants q and p are

$$q = \sqrt{\frac{3}{2}s_{ij}s_{ji}} \quad \text{and} \quad p = \frac{1}{3}\sigma_{kk} \tag{3}$$

where σ_{ij} is the stress tensor and s_{ij} denotes the deviatoric stress tensor. The flow potential was defined as

$$g_1 = q + p\tan\psi \tag{4}$$

where ψ is the dilatancy angle *($\psi \neq \varphi$)*. For the sake of simplicity, the constant values of φ and ψ were assumed.

In turn, in a tensile regime, a Rankine criterion was used with a yield function f_2 with isotropic softening defined as (Marzec *et al.* 2007. Majewski *et al.* 2008, Tejchman and Bobiński 2013)

$$f_2 = \max\{\sigma_1, \sigma_2, \sigma_3\} - \sigma_t(\kappa_2) \tag{5}$$

where σ_i – the principal stress, $\sigma_t(\kappa_2)$ – the tensile yield stress and κ_2 – the softening parameter equal to the maximum principal plastic strain ε_1^p. The associated flow rule was assumed. The edges and vertex of the Rankine yield function were taken into account by the interpolation of 2-3 plastic multipliers according to the Koiter's rule. The same procedure was adopted in the case of combined tension (Rankine criterion) and compression (Drucker-Prager criterion).

This simple isotropic elasto-plastic model for concrete (Eqs. (1)-(5)) requires two elastic parameters: modulus of elasticity E and Poisson's ratio υ, one compression yield stress function $\sigma_c = f(\kappa_1)$ (based on a uniaxial compression test), one tensile yield stress function $\sigma_t = f(\kappa_2)$ (based on a uniaxial tension test), internal friction angle φ and dilatancy angle ψ (based on a triaxial compression test). The model has some disadvantages. The shape of the failure surface in a principal stress space is linear (not paraboloidal as in reality). In deviatoric planes, the shape is circular (during compression) and triangular (during tension); thus it does not gradually change from a curvilinear triangle with smoothly rounded corners to nearly circular with increasing pressure. The strength is similar for triaxial compression and extension, and the stiffness degradation due to strain localization and non-linear volume changes during loading are not taken into account.

3.2 Isotropic damage model for concrete

A simple isotropic damage continuum model was used (Marzec *et al.* 2007, Tejchman and Bobiński 2013) which describes the material degradation with the aid of only a single scalar damage parameter D growing monotonically from zero (undamaged material) to one (completely damaged material). The stress-strain function was represented by relationship (Simo and Ju 1987)

$$\sigma_{ij} = (1 - D) C^e_{ijkl} \varepsilon_{kl} \tag{6}$$

where: C^e_{ijkl} - the linear elastic material stiffness matrix (including modulus of elasticity E and Poisson's ratio υ) and ε_{kl} - the total strain tensor. The damage parameter D acts as a stiffness reduction factor (the Poisson ratio is not affected by damage). The growth of damage is controlled by a threshold parameter κ which is defined as a maximum of the equivalent strain measure $\tilde{\varepsilon}$ reached during the load history up to time t. The loading function of damage was

$$f(\tilde{\varepsilon}, \kappa) = \tilde{\varepsilon} - \max(\kappa, \kappa_0) \tag{7}$$

where κ_0 denotes the initial value of κ when damage begins. If the loading function f is negative, damage does not develop. During monotonic loading, the parameter κ grows (it coincides with $\tilde{\varepsilon}$) and during unloading and reloading it remains constant. The model cannot realistically describe irreversible deformations and volume changes (Simone and Sluys 2004).

We investigated 3 different equivalent strain measures $\tilde{\varepsilon}$. First a Rankine failure type criterion by Jirásek and Marfia (2005) was assumed

$$\tilde{\varepsilon} = \frac{1}{E} \max\left(\sigma_i^{eff}\right) \tag{8}$$

where σ_i^{eff} are the principal values of the effective stress tensor. Second, a modified von Mises definition was adopted (de Vree *et al.* 1995, Peerlings *et al.* 1998)

$$\tilde{\varepsilon} = \frac{k-1}{2k(1-2\upsilon)} I_1^{\varepsilon} + \frac{1}{2k}\sqrt{\frac{(k-1)^2}{(1-2\upsilon)^2}(I_1^{\varepsilon})^2 + \frac{12k}{(1+\upsilon)^2} J_2^{\varepsilon}} \tag{9}$$

where I_1^{ε} is the first invariant of the total strain tensor, J_2^{ε} is the second invariant of the deviatoric strain tensor and k stands for the ratio between the compressive and tensile strength of the material. Third, a criterion following Häußler-Combe and Pröchtel (2005), based on the failure condition by Hsieh-Ting-Chen (Hsieh *et al*. 1982), was chosen

$$\tilde{\varepsilon} = \frac{1}{2}\left(c_2\sqrt{J_2^{\varepsilon}} + c_3\varepsilon_1 + c_4 I_1^{\varepsilon} + \sqrt{\left(c_2\sqrt{J_2^{\varepsilon}} + c_3\varepsilon_1 + c_4 I_1^{\varepsilon}\right)^2 + 4c_1 J_2^{\varepsilon}} \right) \tag{10}$$

with ε_1 - the maximum principal total strain, c_1, c_2, c_3 and c_4 - the coefficients depending on $\alpha_1=f_t/f_c$ (ratio between uniaxial tensile strength and uniaxial compressive strength), $\alpha_2=f_{bc}/f_c$ (ratio between biaxial and uniaxial compressive strength), α_3 and γ – multipliers of material strength in triaxial compression.

To describe the evolution of the damage parameter D, an exponential softening law was chosen (Peerlings *et al*. 1998)

$$D = 1 - \frac{\kappa}{\kappa_0}\left(1 - \alpha + \alpha e^{-\beta(\kappa-\kappa_0)}\right) \tag{11}$$

with α and β as the material constants.

The damage evolution law determines the shape of the softening curve. The material softening starts when the equivalent strain measure reaches the initial threshold κ_0 (material hardening is neglected). With increasing parameter α (usually in the range of 0.7 up to 0.95), both the maximum and residual strength increase. The smaller the parameter β, the higher is the strength and material ductility. For one-dimensional problems, at $\varepsilon\to\infty$ (uniaxial tension), the stress approaches the value of $(1 - \alpha)E\kappa_0$.

The constitutive isotropic damage model for concrete requires 5 material parameters: E, υ, κ_0, α and β (Eq. (8)), 6 material parameters: E, υ, κ_0, α, β and k (Eq. (9)) or 9 material parameters E, υ, κ_0, α, β, α_1, α_2, α_3 and γ (Eq. (10)). The model is mainly suitable for tensile failure. However, it cannot realistically describe irreversible deformations, volume changes and shear failure.

3.3 Anisotropic smeared crack model for concrete

In a smeared crack approach, a discrete crack is represented by cracking strain distributed over a finite volume (de Borst and Nauta 1985, de Borst 1986, Rots and Blaauwendraad 1989). The model is capable of properly combining crack formation and a behaviour of concrete between cracks and of handling secondary cracking owing to rotation of the principal stress axes after primary crack formation. A secondary crack is allowed if the major principal stress exceeds tensile strength and if the angle between the primary crack and secondary crack exceeds a threshold angle. Since the model takes into account the crack orientation, it reflects the crack-induced anisotropy.

The total strains ε_{ij} are decomposed into the elastic ε_{ij}^{e} and inelastic strains ε_{ij}^{cr}

$$\varepsilon_{ij} = \varepsilon_{ij}^{e} + \varepsilon_{ij}^{cr} \tag{12}$$

The stresses are related to the elastic strains by the following relationship

$$\sigma_{ij} = C_{ijkl}^{e} \varepsilon_{kl}^{e} \tag{13}$$

Between the stresses and the crack strains, the following relationship is assumed (in a local coordinate system)

$$\sigma_{ij} = C_{ijkl}^{cr} \varepsilon_{kl}^{cr} \tag{14}$$

with the secant diagonal stiffness matrix C_{ijkl}^{cr} for the cracked concrete (defined only for open cracks). A crack is created when the maximum tensile stress exceeds the tensile strength f_t. To define softening in the normal direction under tension, the relationship by Hordijk (1991) is adopted

$$\sigma_t(\kappa) = f_t\left(\left(1 + (A_1\kappa)^3\right)\exp\left(-A_2\kappa\right) - A_3\kappa\right) \tag{15}$$

with

$$A_1 = \frac{b_1}{\varepsilon_{nu}}, \quad A_2 = \frac{b_2}{\varepsilon_{nu}}, \quad A_3 = \frac{1}{\varepsilon_{nu}}\left(1 + b_1^3\right)\exp\left(-b_2\right) \tag{16}$$

where ε_{nu} is the ultimate crack strain in tension and the material constants are b_1=3.0 and b_2=6.93. The shear modulus G is reduced by the shear retention factor β according to Rots and Blaauwendraad (1989)

$$\beta = \left(1 - \frac{\varepsilon_i^{cr}}{\varepsilon_{su}}\right)^p \tag{17}$$

where ε_{su} is the ultimate crack strain in shear and p is the material parameter. Combining Eqs. (12)-(14), the following relationship between stresses and total strains (in a local coordinate system) is derived

$$\sigma_{ij} = C_{ijkl}^{s} \varepsilon_{kl}\,, \tag{18}$$

with the secant stiffness matrix C_{ijkl}^{s} as

$$C_{ijkl}^{s} = C_{ijkl}^{e} - C_{ijrs}^{e}\left(C_{rstu}^{e} + C_{rstu}^{cr}\right)^{-1} C_{tukl}^{e}\,. \tag{19}$$

After cracking, the isotropic elastic stiffness matrix is replaced by the orthotropic one. Two different formulations were investigated: a rotating crack model and a fixed orthogonal crack model. In the first approach (rotating crack), only can crack is created (softening is defined in one direction only) which could rotate during deformation. To keep the principal axis of total strains and stresses aligned, the secant stiffness coefficient is calculated according to

$$C^s_{ijij} = \frac{\sigma_{ii} - \sigma_{jj}}{2(\varepsilon_{ii} - \varepsilon_{jj})} \tag{20}$$

The second formulation (with a fixed crack) allows one for the formation of three mutually orthogonal cracks in 3D-problems (or 2 orthogonal cracks in 2D simulations). The orientation of the crack is described by its primary inclination at the onset (the crack cannot rotate during deformation).

The constitutive smeared crack model for concrete requires the following 6-8 material constants: E, v, f_t, p, b_1, b_2, ε_{su} and ε_{nu} (fixed crack model) or E, v, f_t, b_1, b_2, and ε_{nu} (rotating crack model). The parameters f_t, b_1, b_2 and ε_{nu} determine the softening behaviour of concrete under uniaxial tension. The values of ε_{su} and p affect the shear retention factor in a fixed crack model. The smaller ε_{su} and larger p, the lower is the effective shear modulus. The model does not allow for permanent deformations, although plasticity may be coupled with it (de Borst 1986).

3.4 Coupled elasto-plastic-damage model for concrete

The model (Marzec and Tejchman 2012) combines elasto-plasticity with a scalar isotropic damage assuming a strain equivalence hypothesis according to Pamin and de Borst (1999). The elasto-plasticity was defined in terms of effective stresses according to

$$C^{eff}_{ij} = C^e_{ijkl}\varepsilon_{kl} \tag{21}$$

In an elasto-plastic regime, a linear Drucker-Prager criterion with a non-associated flow rule in compression and a Rankine criterion with an associated flow rule in tension (Section 3.1) defined by effective stresses were used. Next, the material degradation was calculated within damage mechanics, independently in tension and compression using one equivalent strain measure $\tilde{\varepsilon}$ proposed by Mazars (1986) (ε_i - principal strains)

$$\tilde{\varepsilon} = \sqrt{\sum_i \langle \varepsilon_i \rangle^2} \tag{22}$$

In tension the damage parameter D_t was defined with the same exponential damage evolution function by Peerlings *et al.* (1998) as in the isotropic damage model (Eq. (11)). In turn, in compression, the definition by Geers (1997) was adopted

$$D_c = 1 - \left(1 - \frac{\kappa_0}{\kappa}\right)\left(0.01\frac{\kappa_0}{\kappa}\right)^{\eta_1} - \left(\frac{\kappa_0}{\kappa}\right)^{\eta_2} e^{-\delta(\kappa - \kappa_0)} \tag{23}$$

where η_1, η_2 and δ are the material constants. Eq. (22) allows for distinguishing different stiffness degradation under tension and compression. Damage under compression starts to develop later than under tension according to the experimental behaviour. The stress-strain relationship was represented by following formula

$$\sigma_{ij} = (1 - D)\sigma_{ij}^{eff} \tag{24}$$

where the term '1-*D'* was defined as in Abaqus (2004) following Lee and Fenves (1998)

$$(1 - D) = (1 - s_c D_t)(1 - s_t D_c) \tag{25}$$

with two splitting functions s_t and s_c controlling the magnitude of damage

$$s_t = 1 - a_c w(\boldsymbol{\sigma}^{eff}) \quad \text{and} \quad s_c = 1 - a_t\left(1 - w(\boldsymbol{\sigma}^{eff})\right) \tag{26}$$

where a_t and a_c are the scale factors and $w(\boldsymbol{\sigma}^{eff})$ denotes a stress weight function, which may be determined with the aid of principal effective stresses (Lee and Fenves 1998)

$$w(\boldsymbol{\sigma}^{eff}) = \begin{cases} 0 & \text{if } \sigma_{ij}^{eff} = 0 \\ \dfrac{\sum\langle\sigma_i^{eff}\rangle}{\sum\left|\sigma_i^{eff}\right|} & \text{otherwise} \end{cases}. \tag{27}$$

For relatively simple cyclic tests (e.g. uniaxial tension, bending), the scale factors a_t and a_c can be $a_t = 0$ and $a_c = 1$, respectively. Thus, the splitting functions are: $s_t = 1.0$ and $s_c = w(\boldsymbol{\sigma}^{eff})$. For uniaxial loading cases, the stress weight function becomes

$$w(\sigma^{eff}) = \begin{cases} 1 & \text{if } \sigma^{eff} > 0 \\ 0 & \text{if } \sigma^{eff} \le 0 \end{cases}. \tag{28}$$

Thus, under pure tension the stress weight function w=1.0 and under pure compression w=0. The constitutive model with a different stiffness in tension and compression and a positive-negative stress projection operator to simulate crack closing and crack re-opening is thermodynamically consistent. It shares the main properties of the model by Lee and Fenves (1998), which was proved to not violate thermodynamic principles (with plasticity defined in the effective stress space, isotropic damage and similar stress weight functions). Moreover Carol and Willam (1996) showed that for damage models with crack-closing-re-opening effects included, only isotropic formulations did not suffer from spurious energy dissipation under non-proportional loading (in contrast to anisotropic ones).

The coupled elasto-plastic-damage model requires the following 12 material constants E, υ, κ_0, α, β, η_1, η_2, δ, a_t, a_c, ψ and φ and 2 hardening yield stress functions (the function by Rankine in tension and the function by Drucker-Prager in compression) (Marzec and Tejchman 2012). In the case of linear hardening, 16 material constants are totally needed: E, υ, κ_0, α, β, η_1, η_2, δ, a_t, a_c, ψ, φ, initial yield stresses σ_{yt}^0 and σ_{yc}^0 and hardening plastic moduli H_p (one in compression and one in tension). If the tensile failure prevails, the Rankine yield function (without activating the Drucker-Prager criterion) may be used only.

The quantities σ_y^0 (initial yield stress during hardening) and κ_0 are responsible for the peak location on the stress-strain curve and a simultaneous activation of a plastic and damage criterion (usually the initial yield stress in the hardening function σ_{yt}^0 = 3.5 - 6.0 MPa and κ_0 = (8 - 15) × 10^{-5} under tension). The shape of the stress-strain-curve in softening is influenced by the constant β in tension (usually β = 50-800), and by the constants δ and η_2 in compression (usually δ = 50 - 800 and η_2 = 0.1-0.8). The parameter η_2 influences also a hardening curve in compression. In turn, the stress-strain-curve at the residual state is affected by the constant α (usually α = 0.70 - 0.95) in tension and by η_1 in compression (usually η_1 = 1.0-1.2). Since the parameters α and η_1 are solely influenced by high values of κ, they can arbitrarily be assumed for softening materials. Thus, the most crucial material constants are σ_y^0, κ_0, β, δ and η_2. In turn, the scale factors a_t and a_c influence the damage magnitude in tension and compression. In general, they vary between zero and one. There do not exist unfortunately the experimental data allowing for determining the magnitude of a_t and a_c. Since, the compressive stiffness is recovered upon the crack closure as the load changes from tension to compression and the tensile stiffness is not recovered due to compressive micro-cracks, the parameters a_c and a_t can be taken for the sake of simplicity as a_c = 1.0 and a_t = 0 for many different simple loading cases as e.g. uniaxial tension and bending. The equivalent strain measure $\tilde{\varepsilon}$ can be defined in terms of total strains or elastic strains. The drawback of our formulation is the necessity to calibrate constants for activating an elasto-plastic criterion and a damage criterion at the same moment. As a consequence, the chosen initial yield stress σ_y^0 may be higher than this obtained directly in laboratory simple monotonic experiments. The effect of material constants on the cyclic concrete behaviour under compression and bending was shown by Marzec and Tejchman (2012).

3.5 Reinforcement model

To simulate the behaviour of longitudinal reinforcement bars (modelled as one-dimensional truss elements), an elasto-perfect plastic constitutive law was assumed with E_s = 210 GPa (modulus of elasticity) and σ_y^s = 420 MPa (σ_y^s – yield steel stress). The horizontal steel bars were fixed at ends.

Bond between concrete and reinforcement plays a crucial role in structural behaviour. It embraces three major mechanisms: adhesion and friction between concrete and steel surface, and the bearing of reinforcement ribs against concrete. Usually, two types of bond failures can occur, namely, a pull-out failure or splitting failure (den Ulij and Bigaj 1996). The calculations were carried out only with bond-slip using a relationship between the bond shear stress τ_b and slip u

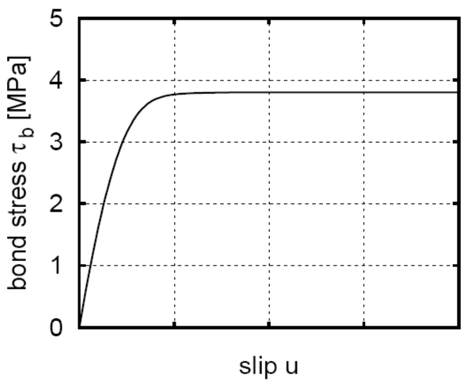

Fig. 2 Bond-slip law between concrete and reinforcement by Dörr (1980)

according to Dörr (1980) due to the fact that bond traction values were far from the limiting value because the bars were fixed at ends. Thus, the shape of the bond law after the peak turned out to be unimportant. To consider bond-slip, an interface with a zero thickness was assumed along a contact, where a relationship between the shear traction and slip was introduced. The bond law by Dörr (1980) neglects softening and assumes a yield plateau (Fig. 2)

$$\tau_b = f_t\left[0.5\left(\frac{u}{u_0}\right) - 4.5\left(\frac{u}{u_0}\right)^2 + 1.4\left(\frac{u}{u_0}\right)^3\right] \quad \text{if} \quad 0 < u \le u_0 \tag{29}$$

$$\tau_b = 1.9 f_t \quad \text{if} \quad u > u_0 \tag{30}$$

where in u_0 is the displacement at which perfect slip occurs. To investigate the effect of the bond stiffness, several numerical tests were carried out with a different values of u_0 changing from 0.06 mm (Dörr 1980) up to 1.0 mm (Haskett *et al.* 2008). It has to be noted that a universal bond law does not exist since it depends on boundary conditions of the entire system (specimen size, concrete type, reinforcement diameter, reinforcement roughness, and confining pressure).

3.6 Non-local approach

To properly describe strain localization, to obtain mesh-independent results and to include a characteristic length of micro-structure for simulations of a deterministic size effect, a non-local theory was used as a regularization technique (Pijauder-Cabot and Bažant 1987, Bažant and Jirásek 2002, Tejchman and Bobiński 2013). In this approach, the principle of a local action does not take place any more. In the calculations within elasto-plasticity, the softening parameters κ_i (i = 1, 2) were assumed to be non-local (independently for both yield surfaces f_i) (Brinkgreve 1994, Bobiński and Tejchman 2004)

$$\bar{\kappa}_i(\boldsymbol{x}) = (1-m)\kappa_i(\boldsymbol{x}) + m\frac{\int_V \omega(\|\boldsymbol{x}-\xi\|)\kappa_i(\xi)d\xi}{\omega(\|\boldsymbol{x}-\xi\|)d\xi} \quad \text{for} \quad i = 1, 2 \tag{31}$$

where $\bar{\kappa}_i(\boldsymbol{x})$ are the non-local softening parameters, V denotes the body volume, $\boldsymbol{x}$ are the coordinates of the considered point, ξ are the coordinates of the surrounding points, ω denotes the weighting function and m is the additional non-locality parameter controlling the size of the localized plastic zone. For m = 1, a classical non-local model is recovered (Pijaudier-Cabot and Bažant 1987). If the parameter $m > 1$, the influence of non-locality increases and a localized plastic region reaches a finite mesh-independent size (Brinkgreve 1994). In the range $0 < m < 1$, mesh-dependent FE results are obtained (Bobiński and Tejchman 2004).

In the calculations within isotropic damage (Section 3.2) and coupled elasto-plastic-damage (Section 3.4), the equivalent strain measure $\tilde{\varepsilon}$ was replaced by its non-local definition (Marzec *et al.* 2007, Marzec and Tejchman 2012)

$$\bar{\varepsilon} = \frac{\int_V \omega(\|\boldsymbol{x}-\xi\|)\tilde{\varepsilon}(\xi)d\xi}{\int_V \omega(\|\boldsymbol{x}-\xi\|)d\xi}. \tag{32}$$

In the smeared crack approach, the secant matrix C^{s}_{ijkl} was calculated with the non-local strain tensor ε_{kl} (independently for all tensor components) according to Jirásek and Zimmermann (1998)

$$\bar{\varepsilon}_{kl}(\boldsymbol{x}) = \frac{\int_V \omega(\|\boldsymbol{x}-\xi\|)\varepsilon_{kl}(\xi)d\xi}{\int_V \omega(\|\boldsymbol{x}-\xi\|)d\xi} . \tag{33}$$

Thus, the resulting stresses were calculated from the relationship

$$\sigma_{ij} = C^{s}_{ijkl}(\bar{\varepsilon}_{kl})\varepsilon_{kl} . \tag{34}$$

As a weighting function ω, the Gauss distribution function was always used (Bažant and Jirásek 2002)

$$\omega(r) = \frac{1}{l_c\sqrt{\pi}} e^{-\left(\frac{r}{l_c}\right)^2} \tag{35}$$

where l_c is the characteristic length of micro-structure and the parameter r is the distance between material points. The averaging in Eq. (35) is restricted to a small representative area around each material point (the influence of points at the distance of $r = 3l_c$ is only of 0.01%). A characteristic length is usually related to the micro-structure of the material (e.g. maximum aggregate size in concrete, grain size in granulates or crystal size in metals). It is determined with an inverse identification process of experimental data (Mahnken and Kuhl 1999, Skarżyński *et al.* 2011). Based on our simulations of concrete and reinforced concrete elements under bending at meso-scale compared to experiments using a digital image correlation DIC technique (Skarżyński and Tejchman 2010, Skarżyński *et al.* 2011, Syroka-Korol 2012), a characteristic length l_c of micro-structure within isotropic elasto-plasticity and isotropic damage mechanics may be about 2 mm (fine-grained concrete) and 5 mm (usual concrete). The setting of a direct relationship between a characteristic length l_c and concrete micro-structure (aggregate size) merits further investigations. In our FE calculations we assumed l_c = 5-20 mm.

The 2D and 3D non-local models were implemented in the commercial finite element code Abaqus (2004) with the aid of the subroutine UMAT (user constitutive law definition) and UEL (user element definition) for efficient computations (Bobiński and Tejchman 2004). For the solution of a non-linear equation of motion governing the response of a system of finite elements, the initial stiffness method was used with a symmetric elastic global stiffness matrix. The calculations were carried out using a large-displacement analysis available in the Abaqus finite element code (Abaqus 2004). According to this method, the current configuration of the body was taken into account. The Cauchy stress was taken as the stress measure. The conjugate strain rate was the rate of deformation. The rotations of the stress and strain tensor were calculated with the Hughes-Winget (1980) method. The non-local averaging was performed in the current configuration. This choice was governed by the fact that element areas in this configuration were automatically calculated by Abaqus (2004).

4. FE input data

The two-dimensional FE calculations were performed with 4 reinforced concrete beams of Section 2 (h = 200 - 800 mm). The characteristic length was l_c = 5 - 20 mm. The regular meshes with quadrilateral elements composed of four diagonally crossed 3-node triangles were used to avoid volumetric locking. The number of triangular elements changed from 2720 (h = 200 mm) up to 16560 (h = 800 mm) The maximum finite element height, 15 mm, and finite element width, 10 mm, were not greater than 3 × l_c to achieve mesh-objective results (Marzec *et al.* 2007). The comparative 3D calculations were performed for the smallest beam of h = 200 mm. The mesh with 16320 eight-node solid elements was used. The maximum sizes of finite elements were again not greater than 3 × l_c (l_c = 10 - 20 mm). The following elastic material parameters were assumed for concrete: E = 28.9 GPa (modulus of elasticity) and υ = 0.20 (Poisson's ratio). The cylinder compressive strength was f_c = 20 MPa and the tensile strength was f_t = 2 MPa. The deformation was induced by prescribing a vertical displacement at the mid-point of the beam top.

5. FE results

5.1 Enhanced elasto-plastic model

Our preliminary FE calculations have shown a certain effect of a characteristic length of micro-structure, compressive fracture energy, tensile fracture energy, softening rate in tension and compression, softening type (linear and non-linear) and stiffness of bond-slip law on both the nominal beam strength, width and spacing of localized zones (Tables 2 and 3). The beam load bearing capacity increased with increasing characteristic length, tensile fracture energy and compressive fracture energy. In turn, the spacing of localized zones increased with increasing characteristic length and softening rate, and decreasing tensile fracture energy, compressive fracture energy and bond stiffness. The calculated width of localized tensile and compressive zones increased with increasing characteristic length l_c and was equal approximately to (1.5 - 4)× l_c with l_c = 5 - 20 mm. The calculated ultimate vertical force V was smaller for the 3D model by 5% only.

On the basis of our preliminary calculations, the further analyses were mainly performed with a 2D model, using a characteristic length of l_c = 5 mm, a non-locality parameter m = 2, and linear softening in compression and tension (Fig. 3). The tensile fracture energy was G_f = 50 N/m and compressive fracture energy was G_c = 1500 N/m. The tensile fracture energy was calculated as $G_f = g_f \times w_f$; g_f – area under the entire softening function (with $w_f \approx 4 \times l_c$ – width of tensile localized zones, l_c = 5 mm). In turn, the compressive fracture energy was calculated as $G_c = g_c \times w_c$ (g_c– area under the entire softening/hardening function up to κ_1 =0.006, $w_c \approx 4 \times l_c$ – width of compressive localized zones, l_c = 5 mm). The internal friction angle was φ=14° (Eq. (2)) and the dilatancy angle was chosen as ψ = 8°. The displacement u_o at which perfect slip occurred was 0.24 mm (Eqs. (29) and (30)). The distribution of material parameters was uniform in all beams.

Fig. 4 shows the calculated force-displacement curves (V – vertical force at the mid-point of the beam top, u – vertical displacement of this mid-point) for the beams of h = 200 - 800 mm. The distribution of the non-local tensile softening parameter $\bar{\kappa}_2$ and non-local compressive softening parameter $\bar{\kappa}_1$ is depicted in Figs. 5 and 6 at the beam failure. In addition, the distribution of $\bar{\kappa}_2$ is shown at the normalized vertical force of $V/(bdf_c)$ = 0.10 as compared to the experimental crack pattern (Fig. 7).

Table 2 Summary of FE-input data

FE-simulat. No.	Beam height h [mm]	Width of tensile localized zones w_f [mm]	Tensile fracture energy G_f [N/m]	Width of compressive localized zones w_c [m]	Compressive fracture energy G_c [N/m]	Charact. length l_c [mm]	Bond model
1a	200	15	50	20	1500	5	bs*
1b		15	50	20	1500	10	
1c		35	50	25	1750	20	
2a	200	15	100	20	1500	5	bs*
2b		20	100	20	1500	10	
2c		40	100	25	1750	20	
3a	200	15	200	20	1500	5	bs*
3b		35	200	25	1750	10	
3c		60	200	25	1750	20	
4a	400	15	50	15	1500	5	bs*
4b		35	50	25	1750	10	
5a	400	20	100	15	1500	5	bs*
5b		40	100	25	1750	10	
6a	600	15	50	15	1500	5	bs*
6b		15	100	25	1750		
7a	800	15	50	15	1500	5	bs*
7b		15	100	25	1750		
8a	200	15	50	20	1500	5	bs*
8b		15	50	20	1500		bs* (u_0=0.12 mm)
8c		15	50	20	1500		bs* (u_0=0.24 mm)
8d		15	50	20	1500		bs* (u_0=1 mm)
9a	400	40	100	25	1750	10	bs*
9b		40	100	25	1750		bs* (u_0=0.12 mm)
9c		40	100	25	1750		bs* (u_0=0.24 mm)
9d		40	100	25	1750		bs* (u_0=1 mm)
10a	200	15	50	20	1500	10	pb*
10b		15	50	20	1500		bs*
11a	400	40	100	25	1750	10	pb*
11b		40	100	25	1750		bs*
12a	200	15	50	15	900	5	bs*
12b		15	50	20	1500		
12c		15	50	20	1800		
13a	400	15	50	20	900	10	bs*
13b		35	50	25	1750		
13c		35	50	25	2250		
14a	200	35	50	25	1750	20	3D, bs*
14b	200	20	100	20	1400	10	3D, bs*
15	200	35	50	25	1750	20	3D, bs*

* bs – bond slip, pb – perfect bond

Table 3 Summary of experiments, FE results and analytical formulae (crack spacing)

FE-simulation No. (Table 1)	Beam height *h* [mm]	Failure vertical force (experiments) [kN]	Failure vertical force (FEM) [kN]	Spacing of localized tensile zones from FEM *s* [mm]	Crack spacing by CEB-FIP model (1991) [mm]	Crack spacing by Lorrain *et al.* (1998) [mm]
1a	200	165	182	105	270	193
1b			185	105		
1c			187	160		
2a	200	165	186	80	270	193
2b			190	80		
2c			193	160		
3a	200	165	190	105	270	193
3b			192	105		
3c			197	160		
4a	400	270	285	180	303	210
4b			287	145		
5a	400	270	291	60	303	210
5b			295	90		
6a	600	350	400	110	337	227
6b			405	170		
7a	800	365	425	85	303	240
7b			435	150		
8a	200	165	182	105	270	193
8b			178	105		
8c			187	105		
8d			175	105		
9a	400	270	295	145	303	210
9b			296	145		
9c			297	145		
9d			275	230		
10a	200	165	195	80	270	193
10b			190	80		
11a	400	270	305	145	303	210
11b			295	180		
12a	200	165	170	80	270	193
12b			182	105		
12c			185	80		
13a	400	270	275	360	303	210
13b			295	145		
13c			297	180		
14a	200	165	195	160	270	193
14b			220	80	270	193
15	200	165	175	160	270	193

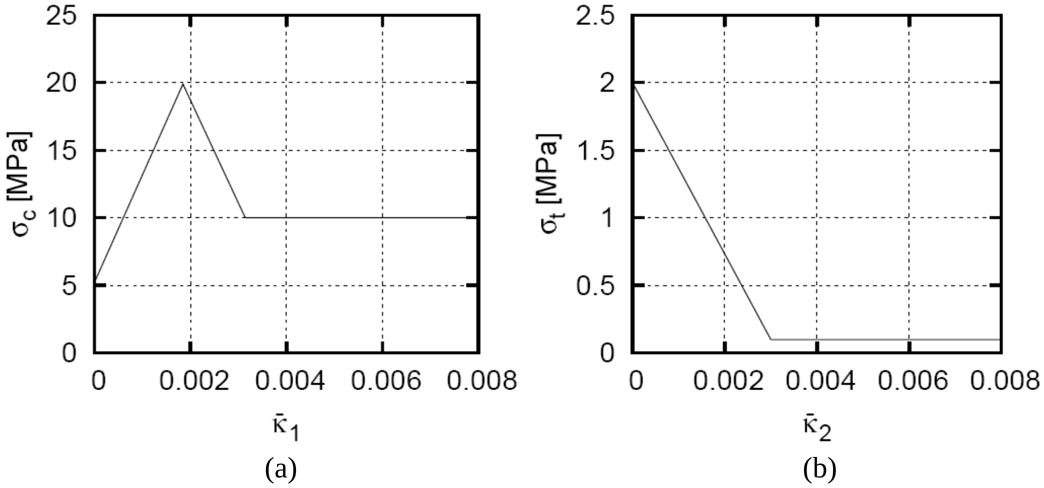

Fig. 3 Assumed hardening/softening functions for elasto-plastic FE calculations: (a) $\sigma_c=f(\bar{\kappa}_1)$ in compression, (b) $\sigma_t = f(\bar{\kappa}_2)$ in tension (σ_t – tensile stress, σ_c – compressive stress, $\bar{\kappa}_i$ – non-local softening parameter)

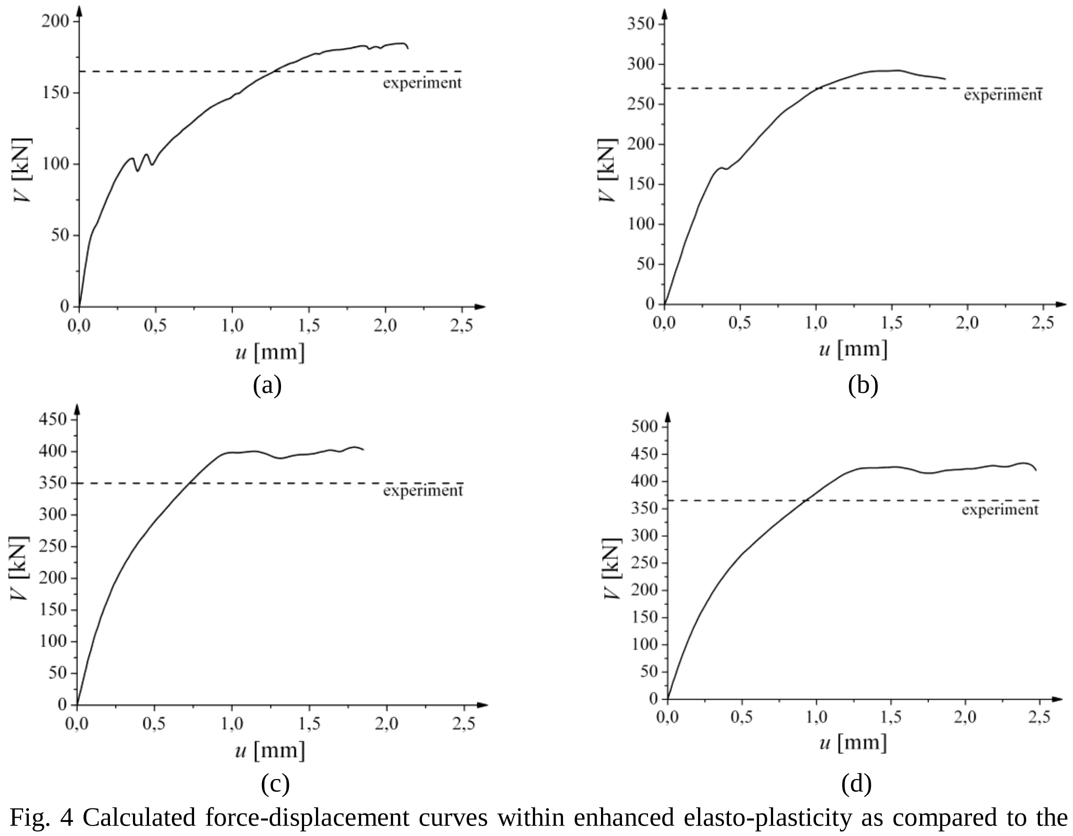

Fig. 4 Calculated force-displacement curves within enhanced elasto-plasticity as compared to the experimental ultimate vertical force for different reinforced concrete beams: (a) h = 200 mm, (b) h = 400 mm, (c) h = 600 mm, (d) h = 800 mm (V – resultant vertical force, u – vertical displacement)

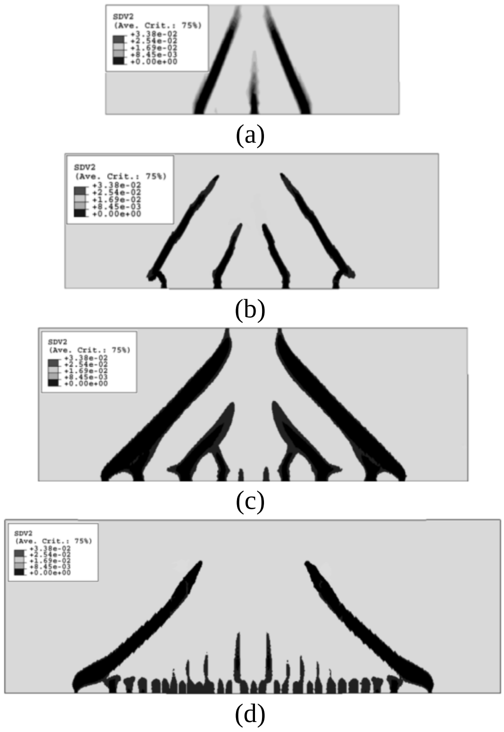

Fig. 5 Distribution of calculated non-local tensile softening parameter $\bar{\kappa}_2$ within elasto-plasticity at failure for different beams: (a) *h*=200 mm, (b) *h*=400 mm, (c) *h*=600 mm, (d) *h*=800 mm (note that beams are not proportionally scaled)

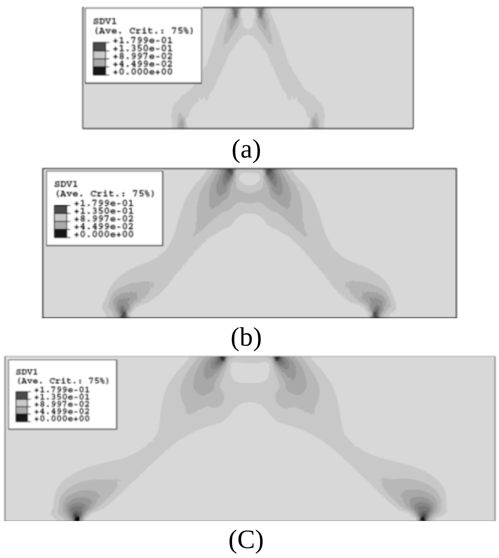

Fig. 6 Distribution of calculated non-local compressive softening parameter $\bar{\kappa}_1$ within enhanced elasto-plasticity for different reinforced concrete beams at vertical displacement of u = 10 mm: (a) h = 200 mm, (b) h = 400 mm, (c) h = 600 mm, (d) h = 800 mm (note that beams are not appropriately scaled)

(d)

Fig. 6 Continued

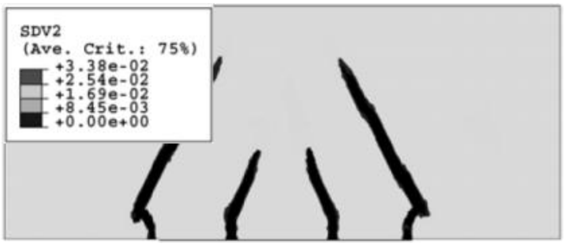

(a) (b)

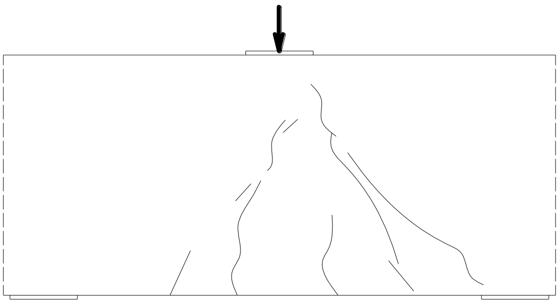

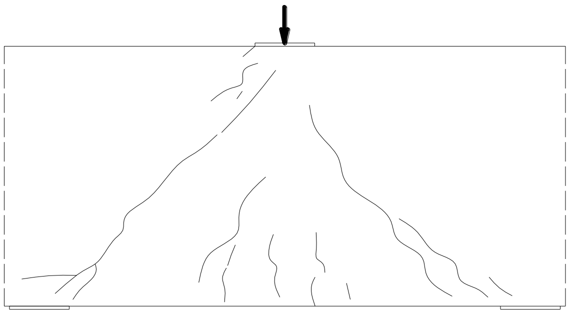

(c) (d)

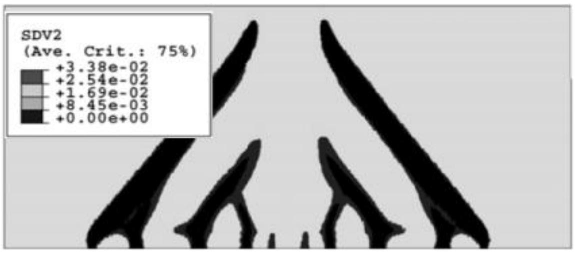

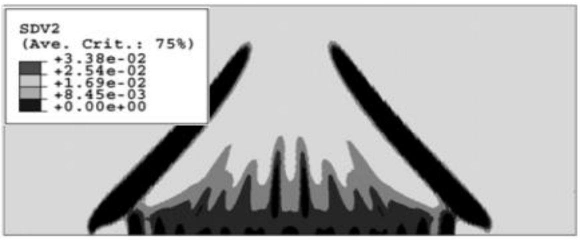

(e) (f)

Fig. 7 Distribution of calculated non-local compressive softening parameter $\bar{\kappa}_2$ within enhanced elasto-plasticity for different reinforced concrete beams at vertical displacement of u = 10 mm: (a) h = 200 mm, (b) h = 400 mm, (c) h = 600 mm, (d) h = 800 mm (note that beams are not appropriately scaled)

The calculated failure forces are in a satisfactory agreement with the experimental ones (Table 3), but are always larger by 10%–20% than the experimental ones (the difference is larger for larger beams). Since a change of material parameters such as l_c, G_f, G_c and u_o have not improved the results (Table 2), it is necessary to use a curved yield surface in compression or to decrease the tensile strength or internal friction angle. The geometry of localized zones matches the experimental crack pattern (Fig. 7), although some differences exist, as e.g. the number of bending localized zones in experiments is smaller than in FE analyses with h = 600 and h = 800 mm. This indicates that too large tensile fracture energy was assumed in calculations. The vertical and inclined long and short localized zones (location and inclination) were numerically well captured. The calculated crack pattern is obviously symmetric in contrast to the experimental one. The widths of calculated tensile and compressive localized zones were about $w_f = w_c = 4 \times l_c$. (Figs. 5 and 6). In turn, the calculated average spacing s of main localized tensile zones was: s = 80 mm (h = 200 mm), s = 90 mm (h = 400 mm), s = 170 mm (h = 600 mm) and s = 150 mm (h = 800 mm), respectively.

The calculated spacing of localized zones s was also compared with the average crack spacing according to CEB-FIP (1990) and Lorrain *et al*. (1998) (see Table 3). The crack spacing by Lorrain *et al.* (1998) is equal to

$$s = 1.5c + 0.1\frac{\phi_s}{\rho} = 1.5\times 32 + 0.1\frac{16}{0.011} = 193\,\text{mm} \qquad (h\text{=200 mm}) \tag{36}$$

$$s = 1.5c + 0.1\frac{\phi_s}{\rho} = 1.5\times 31 + 0.1\frac{18}{0.011} = 210\,\text{mm} \qquad (h\text{=400 mm}) \tag{37}$$

$$s = 1.5c + 0.1\frac{\phi_s}{\rho} = 1.5\times 30 + 0.1\frac{20}{0.011} = 227\,\text{mm} \qquad (h\text{=600 mm}) \tag{38}$$

$$s = 1.5c + 0.1\frac{\phi_s}{\rho} = 1.5\times 51 + 0.1\frac{18}{0.011} = 240\,\text{mm} \qquad (h\text{=800 mm}) \tag{39}$$

where in $\o_s$ = 16 - 20 mm is the mean bar diameter, ρ = 1.1% denotes the reinforcement ratio and c = 30 - 51 mm denotes the concrete cover. The calculated (and experimental) spacing of localized zones, 80 - 170 mm, is significantly smaller than these obtained with the analytical formula by Eqs.3 - 39 (193 - 240 mm).

5.2 Enhanced isotropic damage model

The following parameters were assumed: E = 28.9 GPa, υ = 0.2, κ_0 = 0.0001, α = 0.95 and β = 500, k = 10, α_1 = 0.1, α_2 = 1.16, α_3 = 2.0 and γ = 0.2 (damage approaches by Eqs. (8) - (10)). Figs. 8 and 9 present the results within damage mechanics using the model by Eqs. (8) and (10) (the results using Eq. (9) were similar to those by Eq. (8)).

The force-displacement curves are very similar to those obtained with an elasto-plastic model. The calculated forces at failure are always larger by 2% – 20% than the experimental ones (the difference is greater for a higher beam). To obtain a better accordance, the material constant κ_0 (which is the treshold parameter controling the damage growth) should be smaller. This would cause the damage to develop faster and to decrease the calculated ultimate force. The maximum force decreases also with decreasing material constants α and β (Section 3.2).

Large discrepancies occur in the distribution of localized zones when using an isotropic damage model. A tensile type vertical localized zone at the bottom mid-point was obtained only. The inclined localized zones were not obtained in FE analyses.

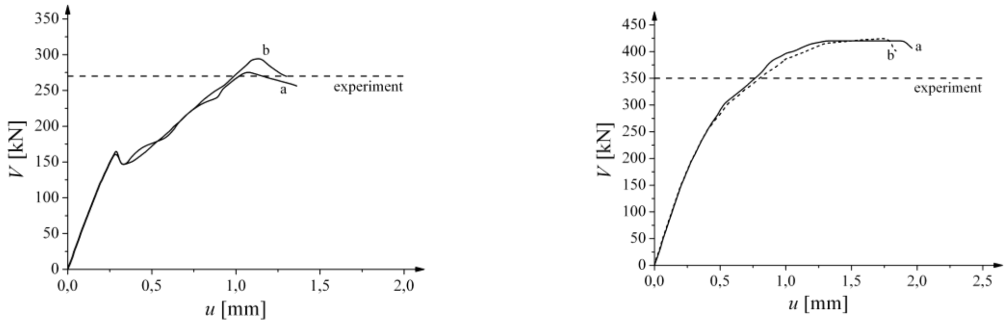

(A) (B)

Fig. 8 Calculated force-displacement curves within enhanced isotropic damage mechanics as compared to experimental maximum vertical force for two reinforced concrete beams: A) h = 400 mm, B) h = 600 mm, (a) equivalent strain measure by Eq. (8), (b) equivalent strain measure by Eq. (10) (V – resultant vertical force, u – vertical displacement)

(A)

(a) (b)

(B)

(a) (b)

Fig. 9 Distribution of calculated non-local equivalent strain measure within enhanced damage mechanics in two reinforced concrete beams at failure: (A) h = 400 mm, (B) h = 600 mm, a) equivalent strain measure by Eq. (8), b) equivalent strain measure by Eq. (10)

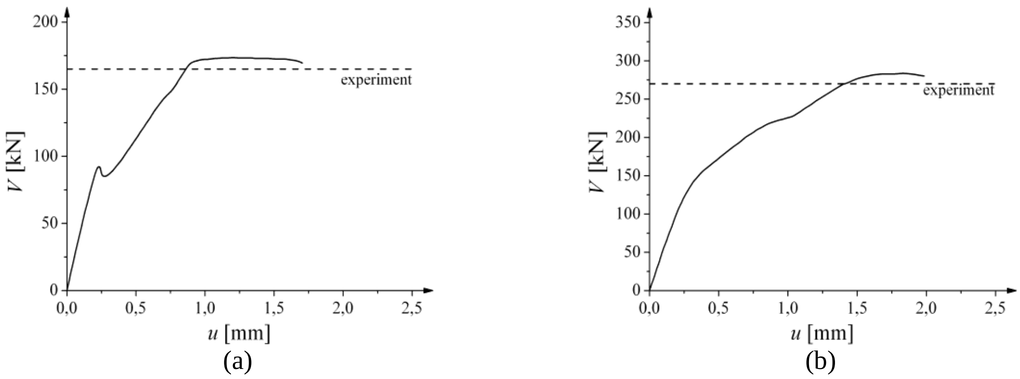

(a) (b)

Fig. 10 Calculated force-displacement curves with enhanced smeared crack approach (as compared to the experimental maximum vertical force) for different reinforced concrete beams: (a) h = 200 mm, (b) h = 400 mm, (c) h = 600 mm, (d) h = 800 mm (V – resultant vertical force, u – vertical displacement)

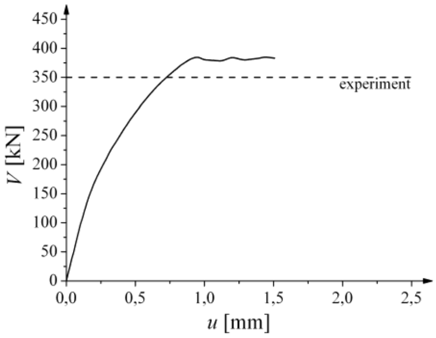

(c)

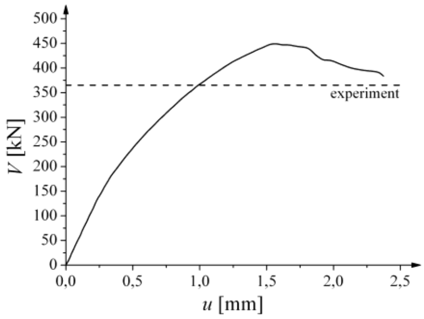

(d)

Fig. 10 Continued

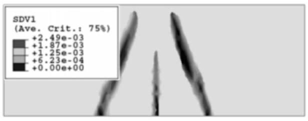

(a)

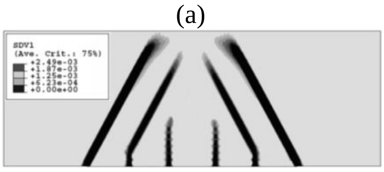

(b)

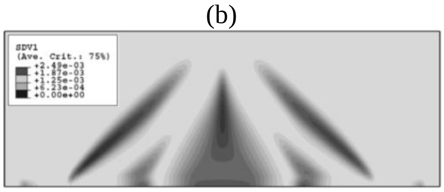

(c)

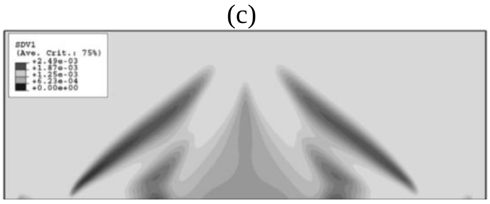

(d)

Fig. 11 Distribution of calculated maximum cracked strain in principal/local direction within enhanced smeared crack approach in different reinforced concrete beams at failure: (a) h = 200 mm, (b) h = 400 mm, (c) h = 600 mm, (d) h = 800 mm (note that beams are not proportionally scaled)

5.3 Enhanced smeared crack model

The following parameters were assumed: E = 28.9 GPa, υ = 0.2, b_1 = 3.0, b_2 = 6.93, f_t = 2.0 MPa, ε_{nu} = 0.006. The results with a smeared rotating crack model are shown in Figs. 10 and 11. The force-displacement curves are very similar to those obtained with an elasto-plastic model. The calculated forces at failure are always larger by 5% - 20% than the experimental ones (the difference increases with increasing beam height). To obtain the lower failure force, plastic deformation should be taken into account (de Borst 1986).

The calculated geometry of localized zones within a smeared crack approach is similar to this within elasto plasticity except of beams with h > 400 mm where the localized zones are more diffuse and a high central bending crack forms. The effect of crack type assumed in the model (fixed or rotating crack model) was insignificant.

5.4 Enhanced coupled elasto-plastic-damage model

The following constants were assumed σyt0 = 3.0 MPa (tension), σ_{yc}^{0} = 30 MPa (compression), Hp=E/2 (in compression and tension), κ_0 = 1.1 × 10 - 4, ϕ = 14°, ψ = 8°, β = 150, α = 0.90, η_1 = 1.1, η_2 = 0.65, δ = 600, a_t = 0 and a_c = 1 (damage was based on elastic strains, l_c = 5 mm). The FE results are given in Figs. 12 and 13. A comparison of results with the coupled model and previous approaches is shown in Fig. 14. Note that the assumed initial tensile yield stresses σ_{yt}^{0} = 3 MPa is different than the uniaxial tensile strength f_t = 2 MPa in the elasto-plastic and smeared crack model due to the enforcement of the simultaneous activation of an elasto-plastic and a damage criterion to simulate both plastic deformation and stiffness degradation (Section 3.4).

The force-displacement curves are quite similar to those obtained with the previous models. The calculated force at failure can be smaller by 3% (h = 200 mm) or higher by 2% (h = 400 mm), 20% (h = 600 mm) and 23% (h = 800 mm) than the experimental one. The largest difference was again for the highest beam. To obtain a better match with respect to the vertical failure force, the material constants σ_{yc}^{0} and κ_0 should be smaller (Section 3.4). In addition, for the lower material

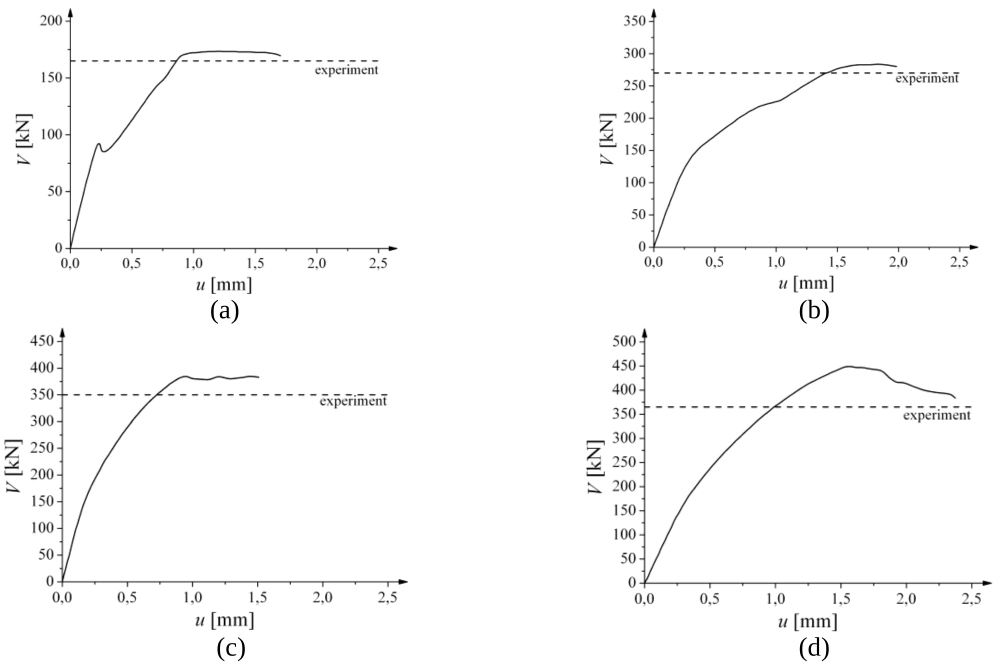

Fig. 12 Calculated force-displacement curves with enhanced coupled elasto-plastic-damage model as compared to experimental maximum vertical force for four different reinforced concrete beams: (a) h = 200 mm, (b) h = 400 mm, (c) h = 600 mm, (d) h = 800 mm (V – resultant vertical force, u – vertical displacement)

constants β, δ and η_2, a more stiffer response of beams in a hardening regime occurred (the effect of η_2 was the most significant). In turn when these constants were higher, beams exhibited a less stiff esponse and a lower failure force. The effect of two other parameters α and η_1 (describing the stress-strain curve at the residual state) on the failure force was negligible.

At the beginning of a loading process, a straight localized zone first occurs in the mid-region, next curved zones are created and finally external the most inclined zones grow and lead to failure. In contrast to elasto-plastic solutions, a central high localized zone always occurs at $h > 200$ mm and a smaller number of localized zones occurs in the mid-region at $h > 400$ mm. The calculated patterns of localized zones within our coupled approach are close to the experimental ones. The inclination of major skew localized zones is similar. The secondary cracks in the central part of the beams are more diffused than in the experiments. The calculated very high localized zone at the beam mid-point was not observed in laboratory tests. The width of the calculated localized zones is roughly $3 \times l_c$. (Fig. 13). In turn, the calculated average spacing s of main localized zones is: s = 80 mm (h = 200 mm), s = 120 mm (h = 400 mm), s = 190 mm (h = 600 mm) and s = 250 mm (h = 800 mm), respectively.

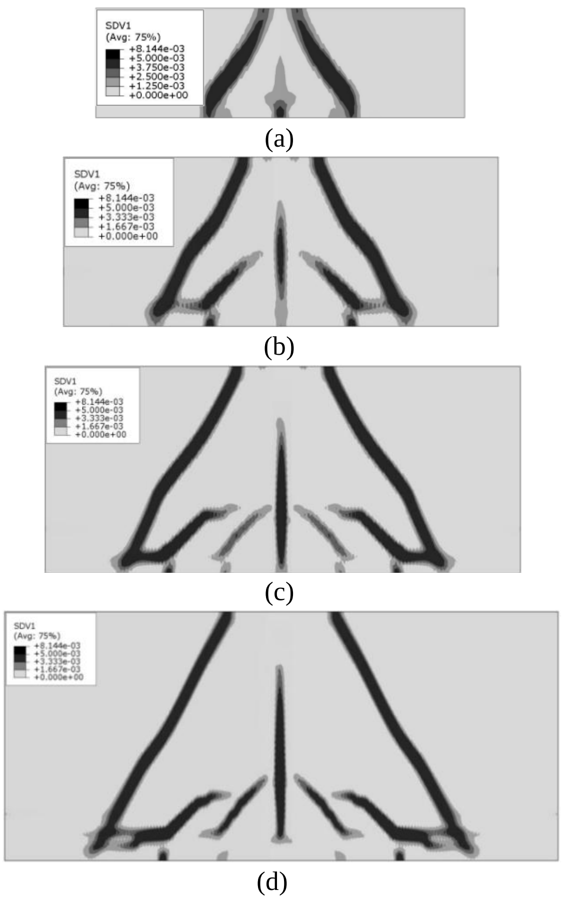

Fig. 13 Distribution of calculated non-local equivalent strain with enhanced coupled elasto-plastic-damage model at failure for four different reinforced concrete beams: (a) h = 200 mm, (b) h = 400 mm, (c) h = 600 mm, (d) h = 800 mm (note that the beams are not proportionally scaled)

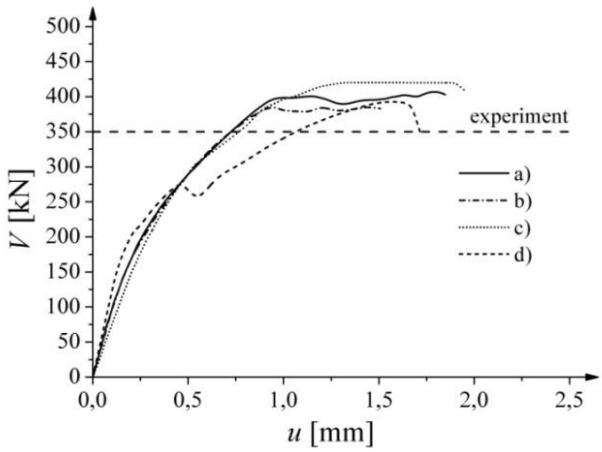

Fig. 14 Calculated force-displacement curves with different models as compared to the experimental ultimate vertical force (beam of h = 600 mm): a) elasto-plastic model b) smeared crack model, d) damage mechanics model and e) coupled elasto-plastic-damage model

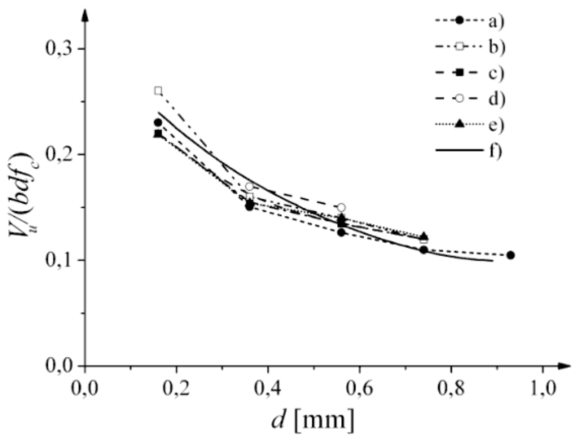

Fig. 15 Calculated size effect in short reinforced concrete beams from FE analyses compared to experiments (Walraven and Lehwalter 1994) and to size effect law by Bažant (Bažant and Planas 1998) (b – beam width, d – effective beam height, f_c – compressive strength of concrete, V_u – ultimate vertical force): a) experiments, b) FE calculations (elasto-plasticity), c) FE calculations (smeared crack model), d) FE calculations (damage mechanics), e) FE calculations (coupled elasto-plastic-damage model), f) size effect law by Bažant

5.4 Deterministic size effect

Fig. 15 shows a comparison between the calculated and experimental size effect: the relative shear stress $V_u/(bdf_c)$ at failure as a function of the effective beam depth. In addition, the size effect law by Bažant (Bažant and Planas 1998) is enclosed. The experimental and theoretical results are close to the size effect law. The experimental and theoretical beam strength shows strong size dependence.

6. Conclusions

The FE-simulations have shown that four different continuum models enhanced by non-local softening are able to realistically capture the behaviour of short reinforced concrete beams without shear reinforcement subjected to shear-tension failure. From the obtained results the following conclusions can be derived:

• The calculated strength of reinforced concrete beams of a different size overestimated the experimental one. The difference increased with increasing beam size (about 20% for the largest beam). Thus, the constitutive models need a further improvement to obtain a better accuracy.

• The geometry of localized zones was in a good agreement within elasto-plasticity and coupled elasto-plasticity and damage, in a medium agreement with a smeared crack approach and completely wrong with isotropic damage mechanics.

• The calculated spacing of localized tensile zones increased with increasing characteristic length, softening rate and beam height and decreasing fracture energy and bond stiffness within elasto-plasticity. The tensile fracture energy was about $G_f = 50$ N/m and compressive fracture energy was $G_c = 1500$ N/m in elasto-plasticity.

• The width of the calculated localized zones was about $(3 - 4) \times l_c$.

• The calculated and experimental spacing of localized zones was significantly smaller than this from available analytical formulae.

• A deterministic size effect was satisfactorily described.

To obtain a better match of FE results with experiments, more refined continuum models could be used. A more advanced concrete model in compression can be implemented in elasto-plasticity (e.g. model proposed by Menetrey and Willam 1995). In addition, the evolution of internal friction and dilatancy against plastic deformation should be taken into account. Within a smeared crack approach, plasticity can be added (de Borst 1986). In the case of a coupled elasto-plastic-damage model, anisotropy may be considered. Other alternative to improve our FE results is to apply macro-continuum models to reinforced concrete elements considered at meso-scale (Gitman *et al*. 2008, Skarżyński and Tejchman 2010).

Acknowledgements

The research work has been carried out within the project: “Innovative ways and effective methods of safety improvement and durability of buildings and transport infrastructure in the sustainable development” financed by the European Union (POIG.01.01.02-10-106/09-01).

The numerical calculations were performed on supercomputers of the Academic Computer Centre in Gdańsk TASK.

References

Abaqus (2004), Theory Manual, Version 5.8, *Hibbit, Karlsson & Sorensen Inc*.

Bažant, Z.P. and Bhat, P.D. (1976), “Endochronic theory of inelasticity and failure of concrete”, *ASCE J. Eng. Mech.,* **102**(4), 701-722.

Bažant, Z.P. and Ožbolt, J. (1990), “Non-local microplane model for fracture, damage and size effect in structures”, *ASCE J. Eng. Mech.*, **116**(11), 2485-2505.

Bažant, Z. and Planas, J. (1998), *Fracture and Size Effect in Concrete and Other Quasi-brittle Materials*, CRC Press LLC.

Bažant, Z.P. and Jirásek, M. (2002), "Numerical integral formulations of plasticity and damage: survey of progress", *ASCE J. Eng. Mech.*, **128**(11), 1119-1149.

Bobiński, J. and Tejchman, J. (2004), "Numerical simulations of localization of deformation in quasibrittle materials within non-local softening plasticity", *Comput. Concr.*, **1**(4), 1-22.

Bobiński, J. and Tejchman, J. (2013), "A coupled continuous-discontinuous approach to concrete elements", *Proceeding of the Int. Conf. Fracture Mechanics of Concrete and Concrete Structures FraMCoS-8*, (Eds. van Mier, J.G.M., Ruiz, G., Andrade, C., Yu, R.C., Zhang, X.X.).

Brinkgreve, R.B.J. (1994), "Geomaterial models and numerical analysis of softening", Ph.D. Thesis, Delft University of Technology, Delft.

Carol, I. and Willam, K. (1996), "Spurious energy dissipation/generation in stiffness recovery models for elastic degradation and damage", *Int. J. Solids Struct.*, **33**(20-22), 2939-2957.

Cervenka, J. and Papanikolaou, V.K. (2008), "Three dimensional combined fracture-plastic material model for concrete", *Int. J. Plasticity*, **24**(12), 2192-2220.

Committé Euro-International du Béton (1991), "CEB-FIP model code 1990: design code", *Bulletin d'inform.*, 213-224.

de Borst, R. and Nauta, P. (1985), "Non-orthogonal cracks in a smeared finite element model", *Eng. Comput.*, **2**(1), 35-46.

de Borst, R. (1986), "Non-linear analysis of frictional materials", Ph.D. Thesis, University of Delft, Delft.

de Borst, R., Pamin, J. and Geers, M. (1999), "On coupled gradient-dependent plasticity and damage theories with a view to localization analysis", *Eur. J. Mech. A/Solids*, **18**(6), 939-962.

de Vree, J.H.P., Brekelmans, W.A.M. and van Gils, M.A.J. (1995), "Comparison of non-local approaches in continuum damage mechanics", *Comput. Struct.*, **55**(4), 581-588.

den Uijl, J.A. and Bigaj, A. (1996), "A bond model for ribbed bars based on concrete confinement", *Heron*, **41**(3), 201-226.

Dörr, K. (1980), "Ein Beitag zur Berechnung von Stahlbetonscheiben unter Berücksichtigung des Verbundverhaltens", Ph.D Thesis, Darmstadt University, Darmstadt , Germany.

Dragon, A. and Mróz, Z. (1979), "A continuum model for plastic-brittle behaviour of rock and concrete", *Int. J. Eng. Sci.*, **17**(2), 121-137.

Geers, M.G.D. (1997), "Experimental analysis and computational modeling of damage and fracture", Ph.D Thesis, Eindhoven University of Technology, Eindhoven, Netherland.

Gitman, I.M., Askes, H. and Sluys, L.J. (2008), "Coupled-volume multi-scale modelling of quasi-brittle material", *Eur. J. Mech. A/Solids*, **27**(3), 302-327.

Haskett, M., Pehlers, D.J. and Mohamed Ali, M.S. (2008), "Local and global bond characteristics of steel reinforcing bars", *Eng. Struct.*, **30**(2), 376-383.

Häuβler-Combe, U. and Pröchtel, P. (2005), "Ein dreiaxiale stoffgesetz fur betone mit normalen und hoher festigkeit", *Beton- Stahlbetonbau*, **100**(1), 56-62.

Hordijk, D.A. (1991), "Local approach to fatigue of concrete", PhD Thesis, Delft University of Technology, Delft, Netherland.

Hsieh, S.S., Ting, E.C. and Chen, W.F. (1982), "Plasticity-fracture model for concrete", *Int. J. Solids Struct.*, **18**(3), 181-187.

Hughes, T.J.R. and Winget, J. (1980), "Finite rotation effects in numerical integration of rate constitutive equations arising in large deformation analysis", *Int. J. Numer. Methods Eng.*, **15**(12), 1862-1867.

Ibrahimbegovic, A., Markovic, D. and Gatuing, F. (2003), "Constitutive model of coupled damage-plasticity and its finite element implementation", *Eur. J. Finite Elem.*, **12**(4), 381-405.

Jirásek, M. and Zimmermann, T. (1998), "Analysis of rotating crack model", *ASCE J. Eng. Mech.*, **124**(8), 842-851.

Jirásek, M. (1999), "Comments on microplane theory", *Mechanics of quasi-brittle materials and structures* (Eds. Pijaudier-Cabot, G., Bittnar, Z. and Gerard, B.), Hermes Science Publications, 55-77.

Jirásek, M. and Marfia, S. (2005), "Non-local damage model based on displacement averaging", *Int. J.*

Numer. Methods Eng., **63**(1), 77-102.
Lee, J. and Fenves, G.L. (1998), "Plastic-damage model for cyclic loading of concrete structures", *ASCE J. Eng. Mech.*, **124**(8), 892-900.
Lorrain, M., Maurel, O. and Seffo, M. (1998), "Cracking behaviour of reinforced high-strength concrete tension ties", *ACI Struct. J.*, **95**(5), 626-635.
Majewski, T., Bobiński, J. and Tejchman, J. (2008), "FE-analysis of failure behaviour of reinforced concrete columns under eccentric compression", *Eng. Struct.*, **30**(2), 300-317.
Mahnken, R. and Kuhl, E. (1999), "Parameter identification of gradient enhanced damage models", *Eur. J. Mech. A/Solids*, **18**(5), 819-835.
Marzec, I., Bobiński, J. and Tejchman, J. (2007), "Simulations of crack spacing in reinforced concrete beams using elastic-plasticity and damage with non-local softening", *Comput. Concrete*, **4**(5), 377-403.
Marzec, I. and Tejchman, J. (2012), "Enhanced coupled elasto-plastic-damage models to describe concrete behaviour in cyclic laboratory tests: Comparison and improvement", *Arch. Mech.*, **64**(3), 227-259.
Mazars, J. (1986), "A description of micro- and macroscale damage of concrete structures", *Eng. Fract. Mech.*, **25**(5-6), 729-737.
Menetrey, P. and Willam, K.J. (1995), "Triaxial failure criterion for concrete and its generalization", *ACI Struct. J.*, **92**(3), 311-318.
Meschke, G. and Dumstorff, P. (2007), "Energy-based modeling of cohesive and cohesionless cracks via X-FEM", *Comput. Meth. Appl. Mech. Eng.*, **196**(21-24), 2338-2357.
Moonen, P., Carmeliet, J. and Sluys, L.J. (2008), "A continuous-discontinuous approach to simulate fracture processes", *Philos. Mag.*, **88**(28-29), 3281-3298.
Oliver, J. and Linero, D.L. and Huespe, A.E. and Manzoli, O.L. (2008), "Two-dimensional modeling of material failure in reinforced concrete by means of a continuum strong discontinuity approach", *Comput. Meth. Appl. Mech. Eng.*, **197**(5), 332-348.
Ooi, E.T. and Yang, Z.J. (2011), "Modelling crack propagation in reinforced concrete using a hybrid finite element–scaled boundary finite element method", *Eng. Fract. Mech.*, **78**(2), 252-273.
Pamin, J. and de Borst, R. (1999), "Stiffness degradation in gradient-dependent coupled damage-plasticity", *Arch. Mech.*, **51**(3-4), 419-446.
Peerlings, R.H.J., de Borst, R., Brekelmans, W.A.M. and Geers, M.G.D. (1998), "Gradient enhanced damage modelling of concrete fracture", *Mech. Cohes.-Frict. Mat.*, **3**(4), 323-342.
Pietruszczak, S., Jiang, J. and Mirza, F.A. (1988), "An elastoplastic constitutive model for concrete", *Int. J. Solids Struct.*, **24**(7), 705-722.
Pijaudier-Cabot, G. and Bažant, Z.P. (1987), "Nonlocal damage theory", *ASCE J. Eng. Mech.*, **113**(10), 1512-1533.
Rabczuk, T. and Zi, G. and Bordas, S. and Nguyen-Xuan, H. (2008), "A geometrically non-linear three-dimensional cohesive crack method for reinforced concrete structures", *Eng. Fract. Mech.*, **75**(16), 4740-4758.
Ragueneau, F., Borderie, Ch. and Mazars, J. (2000), "Damage model for concrete-like materials coupling cracking and friction", *Int. J. Num. Anal. Meth. Geomech.*, **5**(8), 607-625..
Rots, J.G. and Blaauwendraad, J. (1989), "Crack models for concrete, discrete or smeared? Fixed, multi-directional or rotating?", *Heron*, **34**(1), 1-59.
Simo, K.C. and Ju, J.W. (1987), "Strain- and stress-based continuum damage models - I. Formulation", *Int. J. Solids Struct.*, **23**(7), 821-840.
Simone, A. and Sluys, L.J. (2004), "The use of displacement discontinuities in a rate-dependent medium", *Comput. Meth. Appl. Mech. Eng.*, **193**(27-29), 3015-3033.
Skarżyński, Ł. and Tejchman, J. (2010), "Calculations of fracture process zones on meso-scale in notched concrete beams subjected to three-point bending", *Eur. J. Mech. A/Solids*, **29**(4), 746-760.
Skarżyński, L., Syroka, E. and Tejchman, J. (2011), "Measurements and calculations of the width of the fracture process zones on the surface of notched concrete beams", *Strain*, **47**(s1), 319-332.
Sluys, L.J. and de Borst, R. (1994), "Dispersive properties of gradient and rate-dependent media", *Mech. Mater.*, **18**(2), 131-149.

Souza, R.A. (2010), *Experimental and Numerical Analysis of Reinforced Concrete Corbels Strengthened with Fiber Reinforced Polymers*, Computational Modelling of Concrete Structures, (Eds. N. Bicanic, R. de Borst, H. Mang, G. Meschke), *Taylor and Francis Group*, 711-718.

Syroka, E., Bobiński, J. and Tejchman, J. (2011), "FE analysis of reinforced concrete corbels with enhanced continuum models", *Finite Elem. Anal. Des.*, **47**(9), 1066-1078.

Syroka-Korol, E. (2012), "Experimental and theoretical investigations of size effects in concrete and reinforced concrete beams", PhD Thesis, Gdańsk University of Technology, Gdańsk, Poland.

Tejchman, J. and Bobiński, J. (2013), *Continuous and Discontinuous Modeling of Fracture in Concrete Using FEM,* Springer, (Eds. W. Wu and R. I. Borja), Berlin-Heidelberg, Germany.

Walraven, J. and Lehwalter, N. (1994), "Size effects in short beams loaded in shear", *ACI Struct. J.*, **91**(5), 585-593.

CC